

Spectral densities and absorption spectra of the core antenna complex CP43 from photosystem II

Cite as: J. Chem. Phys. **156**, 215101 (2022); <https://doi.org/10.1063/5.0091005>

Submitted: 10 March 2022 • Accepted: 11 May 2022 • Accepted Manuscript Online: 16 May 2022 •
Published Online: 01 June 2022

 Pooja Sarngadharan,  Sayan Maity and  Ulrich Kleinekathöfer

COLLECTIONS

Note: This paper is part of the JCP Special Topic on Photosynthetic Light-Harvesting and Energy Conversion.

 This paper was selected as an Editor's Pick



[View Online](#)



[Export Citation](#)



[CrossMark](#)

ARTICLES YOU MAY BE INTERESTED IN

[The atomistic modeling of light-harvesting complexes from the physical models to the computational protocol](#)

The Journal of Chemical Physics **156**, 120901 (2022); <https://doi.org/10.1063/5.0086275>

[Time-dependent atomistic simulations of the CP29 light-harvesting complex](#)

The Journal of Chemical Physics **155**, 055103 (2021); <https://doi.org/10.1063/5.0053259>

[Computational spectroscopy of complex systems](#)

The Journal of Chemical Physics **155**, 170901 (2021); <https://doi.org/10.1063/5.0064092>

Lock-in Amplifiers
up to 600 MHz



Zurich
Instruments



Spectral densities and absorption spectra of the core antenna complex CP43 from photosystem II

Cite as: J. Chem. Phys. 156, 215101 (2022); doi: 10.1063/5.0091005

Submitted: 10 March 2022 • Accepted: 11 May 2022 •

Published Online: 1 June 2022



View Online



Export Citation



CrossMark

Pooja Sarngadharan,  Sayan Maity,  and Ulrich Kleinekathöfer^{a)} 

AFFILIATIONS

Department of Physics and Earth Sciences, Jacobs University Bremen, Campus Ring 1, 28759 Bremen, Germany

Note: This paper is part of the JCP Special Topic on Photosynthetic Light-Harvesting and Energy Conversion.

^{a)}Author to whom correspondence should be addressed: u.kleinekathoefer@jacobs-university.de

ABSTRACT

Besides absorbing light, the core antenna complex CP43 of photosystem II is of great importance in transferring excitation energy from the antenna complexes to the reaction center. Excitation energies, spectral densities, and linear absorption spectra of the complex have been evaluated by a multiscale approach. In this scheme, quantum mechanics/molecular mechanics molecular dynamics simulations are performed employing the parameterized density functional tight binding (DFTB) while the time-dependent long-range-corrected DFTB scheme is applied for the excited state calculations. The obtained average spectral density of the CP43 complex shows a very good agreement with experimental results. Moreover, the excitonic Hamiltonian of the system along with the computed site-dependent spectral densities was used to determine the linear absorption. While a Redfield-like approximation has severe shortcomings in dealing with the CP43 complex due to quasi-degenerate states, the non-Markovian full second-order cumulant expansion formalism is able to overcome the drawbacks. Linear absorption spectra were obtained, which show a good agreement with the experimental counterparts at different temperatures. This study once more emphasizes that by combining diverse techniques from the areas of molecular dynamics simulations, quantum chemistry, and open quantum systems, it is possible to obtain first-principle results for photosynthetic complexes, which are in accord with experimental findings.

Published under an exclusive license by AIP Publishing. <https://doi.org/10.1063/5.0091005>

I. INTRODUCTION

Photosynthesis, the most important biological process on Earth responsible for converting solar into chemical energy, is assisted by complex photosynthetic machineries in plants, algae, and bacteria. A collective effort of several protein–pigment complexes (PPCs) enables an efficient energy transfer in photosynthetic systems starting with harvesting the solar light and finally leading to charge separation.^{1–3} In oxygenic photosynthesis, photosystem II (PSII) mediates water splitting where molecular oxygen is generated via the oxidation of water.⁴ To do so, the PPCs in PSII establish an energy funnel that enables excitation energy transfer (EET) to the core of the complex.^{5,6} On the structural side, advances in x-ray crystallography have helped in improving the resolution for the PSII core complex (PSII-cc) from *Thermosynechococcus vulcanus* (*T. vulcanus*) from 3.7 to 1.9 Å.^{7,8} As such high resolution structures

reveal the detailed arrangement and orientation of the pigments responsible for the EET, computational studies can help to unravel the molecular details of the underlying physical processes. At the same time, the obtained intricate structure of the PPCs network is complex, and studying the mechanism of energy transfer is challenging. Nevertheless, quite some details of the EET and the charge separation in the dimeric PSII have been revealed over the last years theoretically as well as experimentally.^{9–15} For example, the intertwined correlations between EET and photoprotection in the outer antenna complexes LHCII and some core antenna complexes prompted the need for extensive research and led to several structure-based and time-dependent studies for these peripheral complexes.^{16–20}

The PSII-cc core complex is composed of the four subunits CP43, CP47, D1, and D2 with the corresponding genes PsbC, PsbB, PsbA, and PsbD, respectively. These subunits are positioned in

a dimeric fashion within the thylakoid membrane resulting in a C2 pseudo-symmetry of the complete core complex. The pigment molecules in these PPCs are arranged in such a way that they provide an efficient pathway for the excitation energy to flow to the respective reaction center. How this transfer works in detail at the molecular level is still an open question. For example, it might also be the case that the pigments are arranged such that high robustness is obtained.²¹ The chlorophyll-a (Chl-a) molecules in CP43 and CP47 receive the excitation energy from the peripheral antenna complexes CP26 and LHCII. From CP43 and CP47, the energy flows toward the reaction center of the PSII-cc.⁵ The CP43 complex contains 13 Chl-a molecules whereas CP47 holds 16 pigment molecules. It is interesting to note that the high-resolution structure of the core complex suggests a non-planarity of the chlorin rings in the antenna complexes,⁸ a fact that needs further investigation, especially concerning its consequences for the EET.

In this study, we focus on the excitonic and spectroscopic properties of the CP43 antenna complex from *T. vulcanus*. The pigment molecules in this complex are situated in between coiled-coil protein helix dimers as depicted in Fig. 1. The network of Chl-a molecules is responsible for the energy transfer in the complex as well as its optical and excitonic properties.^{22–25} As one interesting feature of CP43, spectral hole-burning experiments and time-resolved spectroscopy revealed the existence of two quasi-degenerate weakly coupled lowest-energy states.^{26–30} In order to construct the system Hamiltonian and to determine spectroscopic properties theoretically, the weak coupling between the pigments and the two different low energy states needs to be carefully taken into account. In doing so, theoretical calculations for the linear absorption yielded results in good accord with experimental data.^{31,32} For such comparisons between theory and experiment, the corresponding site energies, i.e., the excitation energies between ground and

first excited state, were derived either based on the electrostatics of the complex using the crystal structure or using a refinement thereof including fits to experimental spectra.^{31,32} Note, however, that this fine-tuning of the models using experimental data was done for CP43 complexes of different organisms. Already quite some time ago, efforts were made to calculate the site energies of CP43 based on classical molecular dynamics (MD) simulations combined with the configuration interaction (CIS) method for the excited state energies.³³ A similar approach will also be used in the present investigation but in a much refined manner. Looking into the dynamics of the system is crucial since the structural details of the pigment molecules are continuously altered under the influence of the thermally fluctuating environment.^{15,34} In a complex system such as CP43, each chlorophyll molecule has a slightly different environment impacting the vibrational dynamics of the pigments. Hence, also in this study, a time-dependent view on the protein CP43 is employed based on the molecular details of the complex.

Within the framework of open quantum systems, the impact of the environment on the pigment molecules is described by spectral densities.³⁵ These quantities detail the frequency-dependent exciton–phonon couplings, i.e., the interaction of the primary system and its thermal surrounding. Early studies to compute spectral densities of light-harvesting (LH) complexes in a dynamical fashion employed the CIS approach^{33,36} for the determination of the excited state energies along classical MD trajectories that were then replaced by the numerically much cheaper ZINDO/S-CIS method (Zerner's Intermediate Neglect of Differential Orbital method with spectroscopic parameters)^{36–40} or by DFT calculations (density functional theory).^{41,42} The spectral densities obtained based on classical MD trajectories were, however, problematic in the high-frequency range. Several attempts have been made to overcome the shortcomings of these MD-based models, for example, the geometry mismatch issue,⁴³ which are, on the other hand, partially numerically quite expensive.^{44–49} Recently, we improved the procedure considerably by implementing quantum-mechanics/molecular mechanics (QM/MM) MD simulations instead of purely classical ones yielding promising results.^{20,34,50,51} To this end, we employ the numerically efficient density functional based tight binding (DFTB) method for the dynamics of the pigment molecules while the rest of the system is treated classically.⁵² Subsequently, the excited states of the chromophore molecules are determined using the time-dependent long-range corrected version of the DFTB approach (TD-LC-DFTB) resulting in spectral densities that show a remarkably improved agreement with the experimental counterparts, especially in the high-frequency region.^{20,34,50,51,53} These spectral densities can then serve as key input parameters for the calculation of the exciton dynamics and the optical properties of the respective LH complex.

Unlike determining the absorption spectrum of a single molecule, modeling optical properties of complete LH complexes can be an elaborate task, already for linear absorption spectra. The coupling between the excited states and the vibrational modes of the pigments as well as their environmental modes is essential to obtain a reasonable estimate of the absorption spectra. To incorporate all these couplings between the pigments and their surroundings in the calculation of absorption spectra, one can either employ a formally exact method, such as the hierarchical

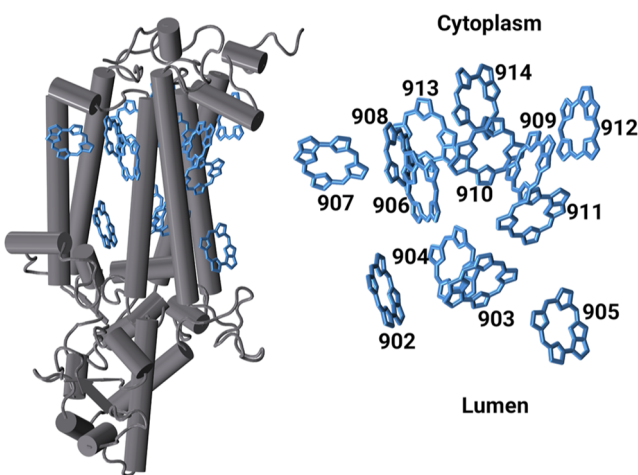


FIG. 1. Left panel: The core antenna complex CP43 represented in cartoon representation with the Chl-a molecules shown in blue (PDB ID: 3WU2). Right panel: Arrangement of the Chl-a molecules in the CP43 protein including their numbering according to the crystal structure. For comparison purposes, the numbering scheme used in Ref. 13 is listed in Table S1.

equations of motion (HEOM) approach^{54,55} or approximative schemes such as perturbative methods.⁵⁶ To this end, perturbative methods have been widely adopted as those are computationally efficient and can be used for large systems. On that account, a cumulant expansion can be used to obtain the line shape function of the excitonic transitions, i.e., of the diagonal elements in the exciton basis. The off-diagonal fluctuations are then treated using different formalisms including the calculation of exciton lifetimes. Probably, the most well-known formalisms in this direction are using Redfield-like equations including the Markovian and sometimes also the secular approximation.^{57–59} The (time-dependent) modified Redfield approximation is another option and has shown to yield improved results in several cases.^{60–62} More recently, the full second-order cumulant expansion (FCE) has been shown to yield rather accurate absorption and circular dichroism spectra of molecular aggregates beyond the Markov approximation and without restrictions on the form of the spectral density.^{63,64} In this study, we will thus employ the FCE scheme for modeling absorption spectra of the CP43 complex at two different temperatures and compare its results with those of a more standard Redfield-like theory and with experimental findings.

II. METHODS

The initial structure of the CP43 complex used for the simulations has been extracted from the high-resolution crystal structure of the PSII-cc from *T. vulcanus* (PDB ID: 3WU2).⁷ The protein, the Chl-a, and the beta carotenoid molecules were taken into account to build the system. All other residual molecules from the crystal structure were removed. Moreover, the missing residues were modeled using the MODELLER suit.⁶⁵ Subsequently, the complex was embedded in a POPC (1-palmitoyl-2-oleyl-sn-glycero-3-phosphocholine) lipid membrane constructed using the Chemistry at Harvard Molecular Mechanics using the CHARMM-GUI web server.⁶⁶ The all-atom force field AMBER03⁶⁷ has been used for the protein and the Lipid-17 force field for the lipid bilayer. In addition, the protein-membrane system was solvated with TIP3P water molecules in a box of dimensions $135 \times 135 \times 127 \text{ \AA}^3$ and neutralized by adding six potassium ions. Finally, the entire system was composed of about 237 K atoms. Furthermore, the ACPYPE (AnteChamber PYthon Parser interface) suite⁶⁸ was employed to generate the topology and coordinates of the whole system in the GROMACS format. Thereafter, the classical MD simulations have been carried out using the GROMACS simulation package, version 5.1.4.

In a first step, we minimized the entire system in a QM/MM fashion using the steepest descent algorithm to remove unfavorable contacts using the GROMACS 2020 together with DFTB+ version 18.2 with a maximum force F_{\max} of $1000 \text{ kJ mol}^{-1} \text{ nm}^{-1}$. In theory, such a procedure should bring the system into the global minimum, while, in practice, one usually ends up in a local minimum (as will be discussed based on the results below). For this QM/MM-optimized conformation, we subsequently determined the Q_y excitation energies using the TD-DFT theory with the CAM-B3LYP functional and def2-TZVP basis set as well as using the TD-LC-DFTB approach (discussed further below). Based on the comparison detailed in Sec. III, it was decided that the simulations along the QM/MM

MD trajectories can be performed using the TD-LC-DFTB scheme (similar to earlier investigations^{20,50,51}).

For further MD simulations, the whole system underwent a classical energy minimization. Subsequently, an NVT equilibration of 2 ns was performed at 300 K to heat up the system with a 1 fs integration time step where position restraints were applied onto the protein, the Chl-a molecules, the β -carotenoids, and the lipid molecules. Moreover, a 20 ns NPT equilibration was carried out with the same restraints. Thereafter, several NPT equilibrations were performed by slowly removing the position restraints. A 10 ns NPT equilibration was run with restraints on the phosphorous atoms of the lipid tails and retaining restraints on the protein, the Chl-a molecules, and the beta carotenoids. In the next step, the restraints on the phosphorous atoms were removed, and a 5 ns NPT equilibration was carried out. In the subsequent NPT equilibrations, the restraints were removed from the β -carotenoids for 5 ns followed by another 5 ns with removing restraints on the chlorophyll molecules but keeping restraints on the magnesium atoms. Up to this step, the integration time step was 1 fs, while for the next equilibration steps, a 2 fs time step was chosen. The subsequent 2 ns NPT equilibration was carried out with restraints on the protein alone. Furthermore, NPT equilibrations with restraints on the side chains of the protein for 2 ns and another 1 ns NPT equilibration with restraints on the $C\alpha$ atoms were carried out to maintain the stability. Finally, a 25 ns NPT equilibration run was performed removing all position restraints.

The isolated CP43 complex underwent a 77 ns-long equilibration in total and led to an intact and stable system. The changes with respect to the initial crystal structure in which the CP43 complex was surrounded by other complexes were small in the trans-membrane helices and somewhat larger in the loop regions of the protein as can be seen in Fig. S1. For this study, more important are the changes in the positions and internal conformations of the Chl-a porphyrin rings. Together with their direct environment, the conformations can directly affect the excited state properties of the complex. Chl-a 903, 905, 912, and 914 show the large shifts of their relative positions after equilibration. The relative shifts in the distance between the magnesium atoms of these Chl-a molecules in the crystal structure and the equilibrated structure are 1.20, 1.74, 1.85, and 1.36 \AA , respectively. The equilibrated system was then subjected to a 200 ns long classical MD simulation and 10 000 snapshots were stored to be used later for the determination of the excitonic couplings.

In the next step, the classically equilibrated structures were used as starting points of QM/MM MD simulations to determine the Q_y excitation energies also known as site energies of each chlorophyll molecule in the CP43 complex. For this purpose, two different starting configurations were extracted from the equilibrated structures for two sets of the 60 ps QM/MM MD simulations. The first frame of the first set has been selected as the final well equilibrated system, whereas for the second set, the initial frame was extracted after an additional 25 ns MD simulation of the equilibrated system. In the QM/MM MD, each of the chlorophyll molecules has been treated separately to get individual site energies due to the limitations in the present implementation. At the same time, this implies that we assume uncorrelated fluctuations of the pigments in these simulations, an assumption that has been tested in detail earlier.^{41,69} For each chlorophyll molecule, the porphyrin ring was

assigned to the QM region with 82 atoms up to the C1 atom and the tail along with the rest of the system was attributed to the MM region. The QM and MM regions are separated by a link-atom scheme using a hydrogen atom. For the QM/MM MD framework, the DFTB3 approach with the 3OB-f parameter set⁷⁰ was used for treating the QM region, whereas the classical AMBER03 force field was employed for the MM region. The usage of the frequency-corrected 3OB-f parameter set is important as the vibrational frequencies of the C=C, C=N, and C=O bond stretching modes are described more accurately leading to an improved description of the vibrational dynamics compared to the 3OB parameter set. The simulations were performed using GROMACS 2020 with DFTB+ version 18.2.^{71,72} Initially, a 20 ps NPT QM/MM equilibration was performed on the two sets at 300 K in the QM/MM setting with a 0.5 fs integration time step. Subsequently, two 60 ps DFTB/MM MD trajectories were generated with the coordinates recorded every 1 fs resulting in two sets of 60 000 snapshots. In addition, an extended simulation with a length of 1 ns was carried out starting from the first set with an integration time step of 1 fs and coordinates stored every 100 fs generating additional 10 000 frames. For all the resulting snapshots from different trajectories, excited state calculations employing the TD-LC-DFTB method with the OB2 parameter set were performed.⁷³ The excitation calculations using TD-LC-DFTB have been benchmarked in previous studies with the computational efficiency of the method being a strong advantage over DFT-based methods.^{20,53} At the same time, in that study,⁵³ the DFT-based approaches have also been tested against wavefunction-based schemes, and a relatively good agreement was found in most cases. For each frame and chlorophyll, the ten lowest-lying excited states were calculated with the help of the DFTB+ package. Subsequently, the Q_y states were carefully extracted along the trajectories. Thereafter, the so-called spectral densities have been determined by performing a cosine transformation of the energy correlational functions. Together with the time-averaged Hamiltonian of the system, these spectral densities have then been used as input to calculate the absorption spectra employing the Redfield and FCE approaches.

III. SITE ENERGY FLUCTUATIONS

The excitonic tight-binding Hamiltonian of the system consists of the site energies E_i of the pigments i and the inter-pigment coupling V_{ij} ,

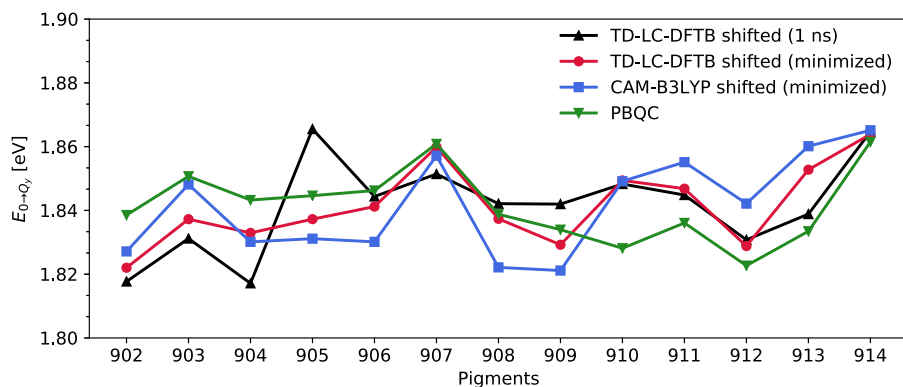


FIG. 2. Average site energies of the Chl-a molecules in the CP43 complex of *T. vulcanus*. Two sets are based on a QM/MM-minimized structure using the TD-LC-DFTB and TD-DFT (CAM-B3LYP) methods. The main result is the average along the 1 ns-long trajectory using the TD-LC-DFTB scheme that is compared with the computed site energies from Müh *et al.*³² of the same organism.

$$H = \sum_i E_i |i\rangle\langle i| + \sum_{i \neq j} V_{ij} |j\rangle\langle i|. \quad (1)$$

This Hamiltonian is defined within the single-exciton manifold; thus, de-excitations to the electronic ground state as well double (and higher) excitations are not included in this model. The excitons move and partially spread within the chlorophyll network and are eventually supposed to find their way to the reaction center, which, however, is not included in this model. To begin the simulation procedure, we calculated the site energies of all 13 Chl-a molecules in the CP43 protein based on a single conformation. To this end, we took the starting frame prepared for the MD simulations, which for the complex itself is very close to the crystal structure and QM/MM minimized it. Based on the resulting conformation, we performed TD-DFT/CAM-B3LYP and TD-LC-DFTB calculations in a QM/MM fashion. Figure 2 shows the resulting site energies compared to those of a previous study on the same organism *T. vulcanus* (pdb: 3WU2). Since we are here only interested in the relative site energies within the CP43 complex, the present results have been shifted to be able to compare the relative trends more easily. To this end, we decided to use the Poisson–Boltzmann/quantum chemical (PBQC) results for *T. vulcanus* from Ref. 32 although these results also include an artificial shift but do lie within a reasonable energy range. The shift is such that for all different approaches in Fig. 2 the site energy average over all pigments is the same as for the calculations by Müh *et al.*³² The TD-DFT values have been shifted by 0.347 eV, the ones for a single conformation using TD-LC-DFTB data by 0.257 eV, and the QM/MM MD 1 ns TD-LC-DFTB site energies by 0.208 eV; the unshifted data are shown in Fig. S2 and the values are given in Table S1 of the supplementary material.

Let us start by comparing the two results for the QM/MM-minimized structure employing two different levels of theory for the excitation energies, i.e., the long-range corrected TD-DFT approach using the CAM-B3LYP functional and the also long-range corrected TD-LC-DFTB scheme that is numerically much more efficient. The observed pattern for the site energies of different pigments is very similar though there are quantitative differences. The agreement between the two DFT approaches found here is consistent with that in a more detailed benchmark study.⁵³ The differences between the results actually wash out to some extent when performing such a comparison not only for a single conformation but also for a whole series of conformations.⁵³ Moreover, the two relative site energy

patterns based on the QM/MM-minimized structure are actually not so different from the results by Müh *et al.*³² on *T. vulcanus*, which were determined based on the Poisson–Boltzmann/quantum chemical (PBQC) method. Again, the overall trend is quite similar despite differences in detail. Overall, the comparison of these three sets of results shows that the numerically very efficient TD-LC-DFTB approach yields quite reliable results for the CP43 complex.

One small caveat is that the calculations by Müh *et al.*³² were done on the basis of the pdb structure 3ARC while the present calculations were performed on the pdb structure 3WU2 that superseded 3ARC. Thus, we looked at the differences for the site energies of similar crystal structures. For *T. vulcanus*, another structure with pdb code 4IL6 exists. Moreover, a structure has been resolved for the CP43 complex of the similar organism *Thermosynechococcus vestitus* BP-1 (*T. vestitus* BP-1 also known as *T. elongatus* BP 1). The site energies are compared in Fig. 3 and one can see that the differences in the site energies of the two structures for *T. vulcanus* are small but non-vanishing. The differences to the site energies of *T. vestitus* BP-1 are, however, larger since this is a different organism and already small differences in a crystal structure can bring about changes in the site energies, especially changes associated with chlorin rings.⁸ For instance, the lowest energy is attributed to Chl-a 904 in *T. vestitus* BP-1 while it is Chl-a 912 in *T. vulcanus*. This finding again highlights that care has to be taken concerning the organism when comparing site energies from different approaches.

As has been shown in many earlier publications,^{1,15,33,74–78} it is not sufficient to determine the excitation energies just for one conformation due to the high flexibility of the light-harvesting complexes at ambient temperatures. Information regarding the site energy fluctuations is crucial in understanding the spectroscopic properties in detail. To this end, the TD-LC-DFTB site energies have been determined for all 13 Chl-a molecules along the 1 ns long QM/MM MD trajectory, as shown in Fig. 4. The site energies of the QM/MM-optimized structure are depicted in this figure as well based on the same level of theory. As is clearly visible, the distributions of the individual pigment molecules differ in their peak position and also in their widths and skewness though all distributions are roughly of Gaussian shape. Moreover, it can be noted that the position of the excitation energies from the so-termed

QM/MM-optimized structure is not at the center of the distribution but in the high-energy wing for all chlorophyll molecules. This finding raises some questions concerning the QM/MM optimization procedure employed since one might have assumed at first sight that the site energies fluctuate around the value for the optimized structure. There are two possible reasons for the off-center positions. First, even if the pigment conformations would fluctuate “perfectly” around a global minimum in the ground-state potential energy surface of the pigments, this does not automatically result in the fact that the excitation energies to the first excited state do fluctuate around the excitation energy for the ground-state minimum conformation. The behavior of the excitation energy distributions does also depend on the excited-state potential energy surface. Even if both surfaces could be assumed harmonic, they would usually be shifted with respect to each other. Second, finding the global minimum with a QM/MM optimization is a non-trivial task and it is not unlikely that the procedure that we performed ended up in a local rather than in the global minimum. As shown in Fig. S3, the conformation after the QM/MM optimization is close to the crystal structure, which also would explain why the site energies for that conformation were similar to those of the results by Müh *et al.*³² The fact that the energies of the QM/MM-optimized conformations are not located closer to the maxima of the respective distributions in Fig. 4 is likely a combination of these two reasons.

The calculations were extended to the two 60 ps QM/MM MD trajectories (with a 1 fs stride), resulting in a site energy pattern almost identical to the one observed for the 1 ns QM/MM MD, as shown in Fig. 5. Thus, the data seem to be reasonably converged. Going back to Fig. 2, one can see that the site energies averaged along QM/MM trajectories show the same trend as the previous calculation for all pigments but for Chl 905. In the other three curves based on the QM/MM-optimized structure and the one showing the results by Müh *et al.*³² pigments 904, 905, and 906 have quite similar site energies. The average site energy for Chl 905 from the QM/MM trajectories has, however, a significantly higher value. Another interesting point for the same pigment is that in the site energy distribution for Chl 905, the energy for the one from the QM/MM-optimized structure is much closer to the peak position of the distributions than is the case for the other sites, as shown in Fig. 4. One can, of course, now raise the question

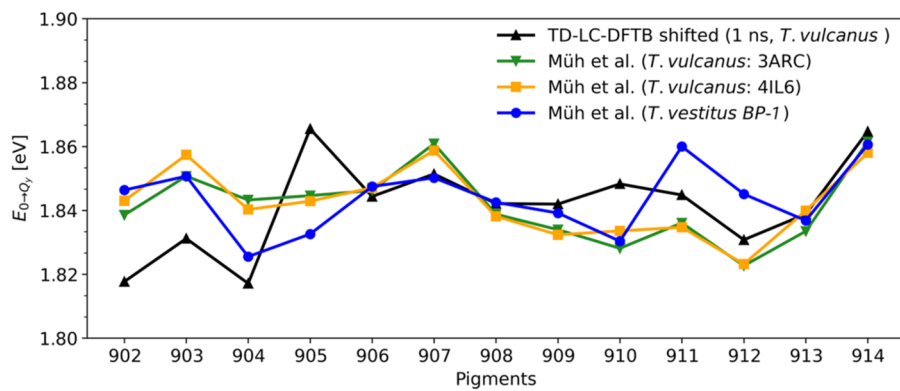


FIG. 3. Average site energies of the Chl-a molecules in the CP43 complex of *T. vulcanus* and *T. vestitus* BP-1. The main result is the average along the 1 ns-long trajectory using the TD-LC-DFTB scheme (*T. vulcanus*), which is compared with the computed site energies from Müh *et al.*³² using the PBQC method from the crystal structures of different cyanobacteria.

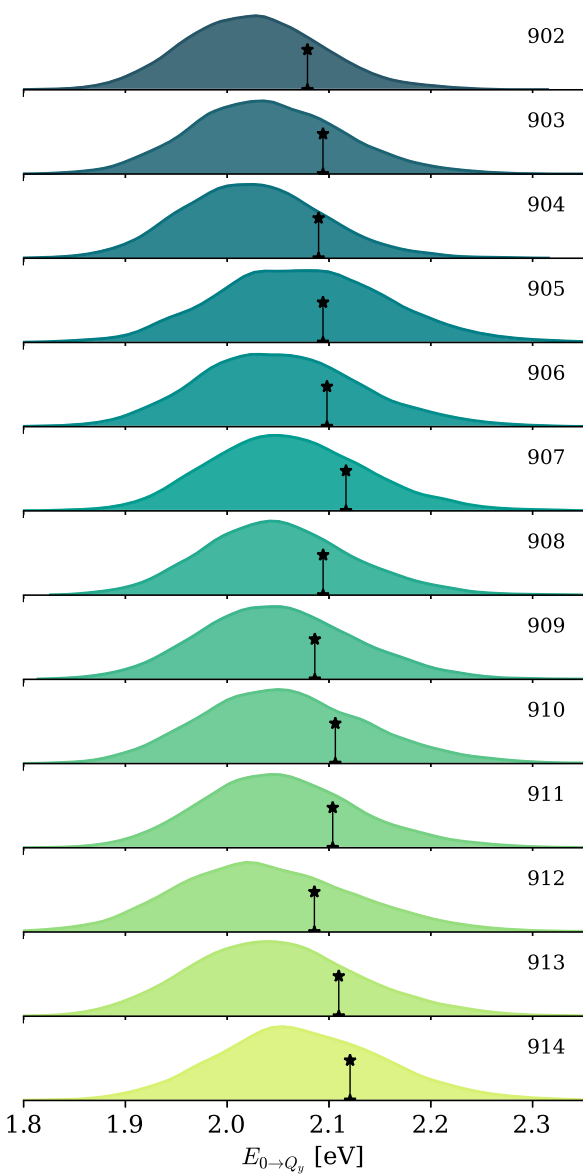


FIG. 4. Distributions of the excitation energy for all Chl-a molecules in the CP43 complex based on the TD-LC-DFTB approach along the 1 ns-long QM/MM MD trajectory. The black markers denote the respective site energies of the QM/MM-minimized structure using the same level of theory.

of which is the “true” site energy for site 905. Looking at the site energy distributions, one clearly sees that the distributions have a much larger standard deviation than the average energetic distance between different pigments. The site energies for the QM/MM-optimized structure all fall into the site energy distribution from the 1 ns dynamics simulation. In the latter case, the lowest energies are found for pigments 902, 904, 912, and 903 in ascending energetic order. In earlier studies, the lowest energy in the CP43 complex was associated with Chl 912,^{30,32} which actually has the largest coupling values to its neighbors among all the pigments as discussed below.

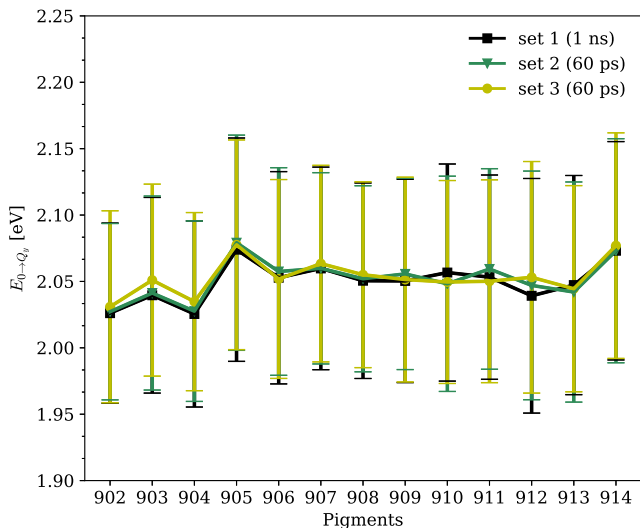


FIG. 5. Average site energies of the Chl-a molecules in CP43 with their standard deviations shown by error bars for the three studied QM/MM MD trajectories.

For the case of the 1 ns QM/MM MD simulation, Chl 912 (2.040 eV) has the second-lowest site energy that is 0.014 eV higher than that of Chl 902 (2.026 eV) and Chl 904 (2.026 eV). Thus, in the present case, Chl 912 has a low but not the lowest site energy.

IV. SPECTRAL DENSITY

Each pigment is embedded in a slightly different protein environment. Hence, the fluctuations in the site energies caused by the (protein) environment are a little different for each chromophore. These variations are already seen in the energy distribution of the site energies as discussed earlier and depicted in Fig. 4. The fluctuations do, however, not only differ in the energy domain but also in the time domain, which can be seen in the Fourier transforms thereof. Quantities that include these transforms are the so-called spectral densities. They provide information about the coupling between the so-called primary modes of the pigment molecules basically representing the electronic excitations into the Q_y state and the environment including vibrational modes of the pigments themselves. Here, we have used a cosine transformation of the site energy auto-correlation functions to calculate the spectral densities of the individual pigments.^{20,36–38} For pigment m , the spectral densities can be computed as

$$J_m(\omega) = \frac{\beta\omega}{\pi} \int_0^\infty dt C_m(t) \cos(\omega t), \quad (2)$$

where $\beta = 1/k_B T$ denotes the inverse temperature and $C_m(t)$ denotes the auto-correlation function at that particular site. In the present case, the latter functions have been obtained from the site energy fluctuations of the 60 ps QM/MM MD trajectories through

$$C_m(t_l) = \frac{1}{N-l} \sum_{k=1}^{N-l} \Delta E_m(t_l + t_k) \Delta E_m(t_k), \quad (3)$$

where ΔE_m denotes the difference of site energy E_m from its average value, i.e., $\Delta E_m = E_m - \langle E_m \rangle$, and N is the total number of frames involved in this calculation. The reorganization energy λ_m of the individual pigment molecules can help to quantify differences and is given by

$$\lambda_m = \int_0^{\infty} \frac{J_m(\omega)}{\omega} d\omega. \quad (4)$$

In the [supplementary material](#) in Table S2, the reorganization energies are tabulated together with variants thereof, which focus on the low frequency region only by reducing the upper limit in the integral in Eq. (4).

The average spectral density averaged over all 13 Chl-a molecules is shown in Fig. 6. Since from experiments no spectral density of CP43 is available, we here compare it to one of the LHCII complexes from fluorescence line narrowing (FLN) experiments, which is supposed to be rather similar.²⁰ For the broadening parameter that controls the broadening of the peaks in the high-frequency region, we used a value of 7 cm^{-1} for calculating the spectral density of LHCII as in our previous study of the complex. As can be seen, the agreement in large parts of the frequency range is very good. In the high-frequency region, the positions and height of several peaks are very similar though certainly not in all cases. The peaks represent intra-molecular vibrational modes involving C=C, C=N, and C=O bond stretching. The agreement in the high-frequency region is especially nice due to the usage of the 3OB-f parameter set within the DFTB3 approach.⁵⁰ Turning off the QM/MM coupling in the excited state calculations, it was shown for a different light-harvesting complex also containing Chl-a molecules that the low-frequency region of the spectral densities represents the influence of the electrostatic environment on the primary modes.³⁹ Due to the similarities of the systems, it is expected that the same is true for the CP43 complex and that the high-frequency contributions in the spectral densities stem from intramolecular vibrations. Moreover, the agreement in the low-frequency region is quite good, and there are several peaks in the range of $200\text{--}400 \text{ cm}^{-1}$, which are almost in line with the experimental counterpart. It seems that

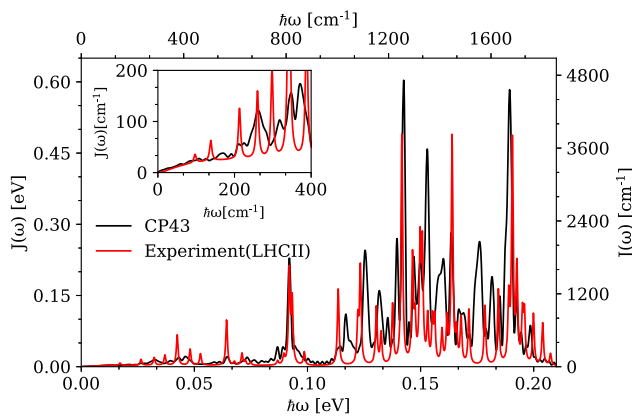


FIG. 6. Calculated average spectral density of CP43 compared with the experimental spectral density obtained from Δ FLN experiments but of LHCII.²⁰

the agreement in the low-frequency range is better when the MM force field in the QM/MM coupling is using a charge model based on real charges such as Amber in the present case or OPLS^{20,51} rather than based on fitting specific interactions as in the case of the CHARMM force field.⁵⁰ A comparison of the average spectral density to that of the CP29 complex together with the individual spectral densities of different pigments are shown in Figs. S4 and S5, respectively.

V. EXCITONIC COUPLING

The excitonic coupling values between the pigments in the CP43 complexes were computed using the transition charges from the electrostatic potential (TrESP) method proposed by Renger and co-workers.^{79,80} The scheme is widely recognized for being accurate and efficient at the same time. Thus, it is routinely being employed to determine the coupling values between pigments that are relatively far apart in antenna complexes.⁵³ In the TrESP approach, the coupling between pigments m and n is given by

$$V_{mn} = \frac{f}{4\pi\epsilon_0} \sum_{I,J}^{m,n} \frac{q_I^T \cdot q_J^T}{|r_m^I - r_n^J|}, \quad (5)$$

where q_I^T and q_J^T denote the transition charges of atoms I and J from the respective donor m and acceptor n molecule. The distance-dependent screening function f takes care of the environmental influences on the excitonic coupling. In this study, we have used an exponential screening factor derived by Curutchet *et al.*⁸¹ given by

$$f(R_{mn}) = A \exp(-BR_{mn} + f_0), \quad (6)$$

where R_{mn} denotes the distance between the centers of the two respective molecules and the parameters A , B , and f_0 have the values 2.68, 0.27, and 0.54, respectively. Since this version of a screening factor takes into account only explicit effects (cavity effect and screening of interaction) but not implicit effects (enhancement of transition dipole moments by environment),⁸² we also list the results using an alternative screening function with a constant value of 0.69 as derived for the PSI system⁸³ in Table S3.

Since QM/MM dynamics simulations with the present implementation can only handle one QM zone at a time and including two pigments into the QM zone is numerically very expensive, we used a 200 ns classical MD trajectory to determine time-averaged coupling values as we have done similarly before for other complexes.^{20,50,51} The site energies are taken from the 1 ns QM/MM MD. According to Eq. (1), the diagonal elements of the Hamiltonian matrix represent the site energies and the off-diagonal elements the couplings. The resulting time-averaged Hamiltonian is listed in Table I. To enable a simpler comparison with the earlier coupling values by Müh *et al.*³¹ for the organism *Thermosynechococcus elongatus*, we included those in the table as well. As can be seen, there are quantitative but no major qualitative differences. Depending on the dipole moments and their orientation in the pigments, the coupling values are either positive or negative. In the CP43 complex, Chl-a 912 has strong couplings with its neighboring chlorophyll molecules 910 and 911. If one wants to extend this cluster of pigments, Chls 910 and 911 have also reasonably large couplings to

TABLE I. Time-averaged system Hamiltonian of the CP43 complex based on exciton coupling values extracted from the 200 ns classical MD trajectory and site energies from the 1 ns QM/MM MD simulation. The site energies and the coupling values (in cm^{-1}) that are above 30 cm^{-1} are shown in boldface. The lower triangle in the table represents the current findings while the upper triangle reproduces the values from Müh et al.³¹ for the different but similar organism *T. elongatus*.

a902	a903	a904	a905	a906	a907	a908	a909	a910	a911	a912	a913	a914
a902 16 341.84	-4.0	-1.0	-0.2	-1.6	8.4	8.7	1.3	-5.0	2.4	-1.1	-0.1	0.3
a903 -6.0	16 450.52	-21.9	40.5	0.6	-4.9	-4.4	1.1	11.9	-8.1	7.0	-4.0	-0.5
a904 4.9	-19.9	16 337.27	-12.1	-1.3	-0.5	-3.0	-2.5	-2.3	-9.1	-3.2	10.1	2.1
a905 -1.4	36.7	-13.3	16 556.84	1.3	2.1	1.3	3.4	-1.4	11.2	1.5	-1.7	1.6
a906 -1.1	0.2	-1.7	1.5	16 613.62	-7.1	-43.3	-8.2	12.0	-1.8	-0.4	1.2	-1.9
a907 4.9	-3.6	-1.0	2.0	-9.5	16 538.74	20.0	6.7	-15.2	7.0	2.3	-3.6	4.3
a908 8.1	-5.1	-3.8	1.2	-39.4	22.4	16 613.62	-5.9	40.9	-1.2	-4.3	18.7	-12.7
a909 0.1	2.4	-2.3	3.3	-6.9	5.9	-6.1	16 537.61	6.1	45.3	22.8	-14.1	5.9
a910 -4.7	13.7	-2.8	-1.4	10.4	-15.9	33.1	15.7	16 588.48	-27.5	63.8	2.3	-2.3
a911 1.1	-2.5	-9.4	13.8	0.1	5.7	0.1	45.1	-42.6	16 560.55	-41.6	-7.1	4.8
a912 -1.4	6.5	-2.7	1.6	-0.04	2.2	-3.2	24.1	66.5	-47.7	16 447.31	-14.4	6.8
a913 -0.1	-4.0	11.4	-1.7	0.4	-5.1	13.6	-13.7	6.4	-5.5	-12.0	16 512.43	-31.1
a914 0.1	-0.8	2.5	1.9	-1.8	4.7	-13.0	5.6	-5.7	4.5	5.3	-14.7	16 720.87

Chls 908 and 909, respectively. Figure 7 shows the coupling fluctuations of pigment pairs with coupling values above 30 cm^{-1} . The distributions are rather symmetric and are relatively Gaussian in nature. All these high coupling values can be attributed to the physical proximity of the involved pigment pairs. At the same time, we want to remark that to our experience including the coupling fluctuations in dynamical simulations does not change the exciton dynamics significantly.^{50,78}

When determining the excitonic states from the whole system Hamiltonian (as shown in Fig. S6), the lowest state is dominated by Chls 904, 902, and 903, as is the case for the second excitonic state. Chl 912 becomes the major contributor to the third excitonic state. From hole burning studies, it is known that the so-called quasi-degenerate weakly coupled energy traps “A” and “B”²⁶ of the complex are localized in two different Chl-a domains. Based on this finding, it has been proposed³¹ to split the CP43 Hamiltonian into two parts one containing Chl 902-903-904-905 and the other one consisting of Chl 906-907-908-909-910-911-912-913 Chl, which

are assumed to be uncoupled since the calculated coupling values between these two pools of pigments are very small. The former pool of Chl-a molecules is located toward the lumen of the thylakoid membrane while the latter one is situated toward the cytoplasmic layer. Upon calculating the excitonic energies from the two separate Hamiltonians for the two sets of pigments, Chl 904 is the major contributor to the lowest energy state followed by Chl 902 in the Chl pool 902-903-904-905. The pigment Chl 912 is the major contributor to the lowest energy state in the second pool. The fairly large coupling values between Chls 910-911-912 lead to a spread of the lowest exciton among these three pigments. In Sec. VI, the spectral densities of the pigments together with the time-averaged Hamiltonian will be used to obtain linear absorption spectra of the CP43 complex at two temperatures.

VI. ABSORPTION SPECTRA OF CP43 COMPLEX

A large variety of methods and approximations exist on how to determine linear absorption spectra for PPCs.^{56,61–63,84} Several studies have tried to compare various approximations from Redfield-like approaches over non-Markovian schemes to the hierarchy equation of motion theory. Here, we adopted two approaches: Redfield-like theory that has frequently been used for PPCs^{58,59,85} and the FCE scheme that neither involves the Markov nor the secular approximation.^{63,64} For linear absorption spectra, the latter approach is actually equivalent to a time-local (time-convolutionless) second-order approach. For spectral densities that can be decomposed into a sum of Lorentzian functions, the results of this scheme have been compared to several other (non-)Markovian theories and to (modified) Redfield theory.⁸⁴

To obtain the absorption spectra of the CP43 system, we used the spectral densities of the individual pigments together with the time-averaged Hamiltonian of the system as given in Table I and the respective transition dipole moments. The transition dipole moment vectors were extracted from the TD-LC-DFTB results of the 1 ns QM/MM MD trajectory and averaged over 10 000 frames by averaging magnitude and direction separately. For the calculation of the

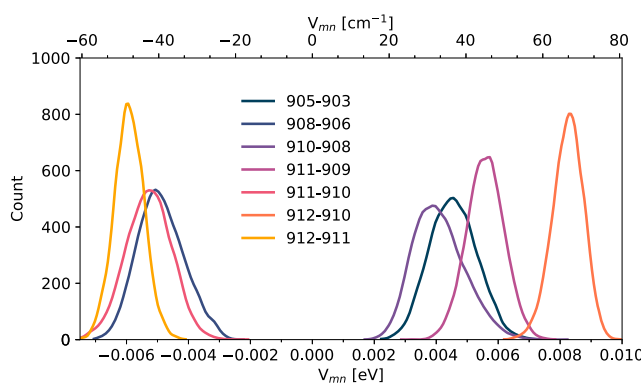


FIG. 7. The distribution of couplings above 30 cm^{-1} calculated from a 200 ns classical MD trajectory using the TrESP method.

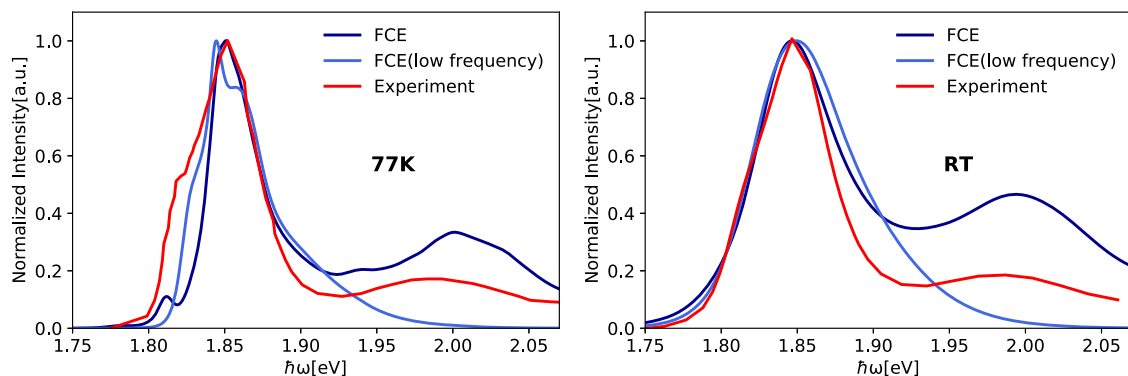


FIG. 8. Absorption spectra of the CP43 complex based on the FCE method compared with experimental spectra from Groot *et al.*²² The FCE data have been shifted by 0.1 eV to lower energies and the FCE using only the low-frequency part of the spectral density by 0.18 eV to lower energies in order to match the position of the main experimental peaks.

absorption spectra at room temperature and at 77 K, we employed the Redfield theory^{58,59} as we already did for the CP29 complex⁵¹ and the FCE method.^{63,64} For the FCE approach, we used a code provided by Cupellini and Lipparini, which can handle arbitrary spectral densities.⁸⁶

Let us start with the results of the FCE scheme. As shown in Fig. 8, the agreement of the calculated absorption spectra with the experimental ones at both temperatures is quite good. The positions of the calculated spectra have been shifted to match those of the experimental ones as is common practice. This shift includes errors in the absolute excitation energies of the pigments where it is assumed that this error is the same for all pigments as well as the so-called reorganization energy shift. The latter shift is included in some theories for absorption spectra such as the modified Redfield approach or some versions of the Redfield formalism but not in the schemes employed here. In particular, the widths of the main peaks in the absorption spectra reasonably well reproduce the experimental findings. Moreover, the relative positions and widths of side bands at higher frequencies are remarkable. To better understand the origin of the side peak, we repeated the calculations with modified spectral densities in which we only included the low-energy part below 0.083 eV (670 cm^{-1}). It is clearly visible in Fig. 8 that in this case the sideband completely disappears. Thus, this sideband emerges due to the high-frequency peaks in the spectral density, which are based on the intra-molecular vibrational dynamics of the pigment molecules. Since these artificial spectral densities have different reorganization energies as the full spectral densities, the so-called reorganization energy shift for the absorption spectra is different. The shift to reproduce the experimental peak position for the truncated spectral density is larger by 0.08 eV. Looking at the data for the reorganization energies in Table S2, this value is similar to the average difference of about 0.095 eV between the reorganization energies for the full and the artificially truncated spectral densities nicely supporting earlier findings.^{87–89} Not perfectly reproduced by the FCE approach is the ratio of the height of the main and the side peak. Assuming that this problem is not an artifact of the FCE formalism, this hints at some problems in the spectral densities.

Specifically, lower peak amplitudes in the high-frequency region or higher amplitudes in the low-frequency region of the spectral density would lead to an improved ratio between the heights of the main peak and the sideband peak. The same would be true if the peaks in the high-frequency region would be a bit narrower, which might actually be a valid option looking at Fig. 6, a point that needs to be further evaluated in future studies.

As an alternative scheme, we want to test the Redfield approach for the determination of linear absorption spectra since it has been used frequently for LH complexes.^{51,58,59,85,90,91} It is to be noted that the effect of coupling fluctuations on the line shape function is neglected here under the assumption that the individual pigments are uncorrelated.⁹¹ The same input parameters for modeling the absorption within the FCE and Redfield approximations were used. The Redfield method resulted in a rather poor line shape compared to the experimental results, as shown in Fig. 9. It had been proposed earlier^{15,64} that Redfield theory does have a problem with this system due to two quasi-degenerate states in this complex, which were observed in experimental studies earlier.^{24,26,28,30} As mentioned already above, the two quasi-degenerate states within the CP43 complex are associated with the fact that there exist two almost separate pools of Chl-a molecules between which the excitonic coupling is rather small. To cure this issue, it was proposed³¹ to split the Hamiltonian into two separate parts neglecting the small coupling between the two pigment pools to determine the absorption separately and then add them up. This procedure leads to an improvement in the spectra, which is, however, not convincing and far worse than the FCE results when comparing to the experimental spectra as shown in Fig. S7. For the FCE approach, this splitting does not make any difference (see Fig. S8). Thus, for the present system, Redfield-like theory fails to deliver accurate absorption spectra and the FCE approach is by far superior though the Redfield theory yields a better ratio between the heights of the main and the side peak. One should keep these problems of Redfield theory in mind when using this approach to fine-tune site energies based on absorption spectra determined using the Redfield approximation.

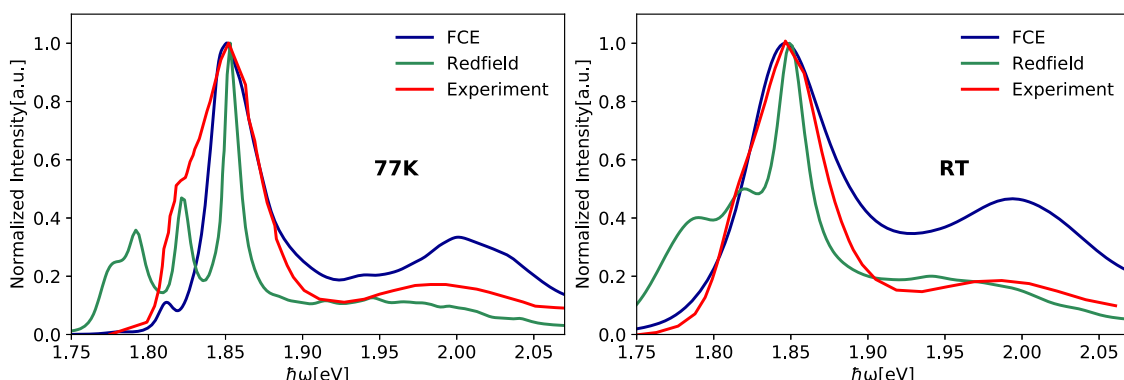


FIG. 9. Absorption spectra of the CP43 complex based on the FCE and Redfield methods compared with experimental spectra from Groot et al.²² The FCE data have been shifted by 0.1 eV toward lower energies and the Redfield data by 0.17 eV in the same direction to match the main experimental peak.

Since we are here comparing to ensemble absorption spectra, it would be sensible to include static disorder in the calculations as well.^{91,92} Unfortunately, a static disorder that is usually included as an additional Gaussian disorder of the site energies is hard to obtain using molecular simulations. One option is to extract uncorrelated snapshots from long-time MD simulations^{56,91,93} with a more detailed approach reported recently.¹⁵ Alternatively, one could also look at many more or less independent simulations of the same pigment–protein complex and try to extract values for the static disorder from there. This approach has recently tried using 63 copies of a light-harvesting II complex within a chromatophore⁹⁴ and sensible estimates for the static disorder were extracted in this way. In this study, we focused on more accurate but also numerically more expensive QM/MM simulations that make extraction of static disorder unfeasible, and thus, we refrained to include it in the present calculations.

VII. CONCLUSIONS

In this study, we have investigated the light-harvesting properties of the core antenna complex CP43 by using a multi-scale strategy. To this end, we combined DFTB/MM MD dynamics with excitation energy calculations using TD-LC-DFTB. The results were thereafter analyzed in terms of averaged site energies including the corresponding fluctuations, site-dependent spectral densities, and finally linear absorption spectra. With this procedure, it was shown that it is possible to determine linear absorption spectra for light-harvesting complexes from first-principles even if the system has some non-trivial features such as quasi-degenerate states.

One of the important points of this study is that not only a single structure has been analyzed but also a complete trajectory. Before doing so, however, the results for a QM/MM-optimized structure were compared for TD-DFT calculations on the CAM-B3LYP and TD-LC-DFTB. Although the results for the latter method, which is numerically much more efficient, were not perfectly matching those of the former approach, the results are quite reasonable and reproduce the site energy pattern well. Thus, the TD-LC-DFTB was employed for the excitation energies as done

before already.^{20,50,51,53} When looking at the average site energies along the QM/MM trajectory, it is surprising to find that the energy of Chl 905 differs significantly from the energies found on single conformations. For all other pigments, the trend is quite similar to that found for the QM/MM-optimized structure. In the next step, the fluctuations of the site energies were analyzed in the energy domain as distributions (density of states) and in the time domain by virtue of the Fourier transform as spectral densities. When the site-dependent spectral densities are averaged over all pigments, one obtains a very nice agreement with the experimental spectral density of the quite similar LHCII complex. Unfortunately, no experimental spectral density is available for the CP43 complex. This first comparison with an experimental finding was already promising.

After constructing a time-averaged Hamiltonian for the complex, it was employed together with the site-dependent spectral densities to determine the linear absorption. If one employs a Redfield-like approach, the absorption spectra include too many peaks even if one employs a trick, which has helped to cure the problem in similar situations.³¹ Employing, however, the FCE scheme that does not involve the Markov or the secular approximation yields line shapes that are quite similar to those found in the experiment. Thus, not only do the spectral densities agree nicely with their experimental counterparts but also the line shapes of the absorption spectra at low and ambient temperatures. One has to keep in mind that these results have been obtained purely based on first-principles, while further improvements both on the methodological and on the implementation level are underway.

The obtained results are promising, especially since the comparison with two independent experimental results, i.e., linear absorption and fluorescence line narrowing, yields very good agreement. The core antenna complex CP43 is, however, only a small part of the whole PSII machinery. This study paves the way to also try to explore larger arrangements of LH complexes though numerically this might still be very challenging. To this end, the study of a complete chromatophore⁸⁵ on the MD level supported by some QM/MM calculations gives some hints of what might come in the future.

SUPPLEMENTARY MATERIAL

See the [supplementary material](#) for extra figures on site energy distributions, spectral densities, and absorption spectra.

ACKNOWLEDGMENTS

Financial support by the Deutsche Forschungsgemeinschaft (DFG) (Grant Nos. KL-1299/18-1 and KL-1299/24-1) was gratefully acknowledged.

AUTHOR DECLARATIONS

Conflict of Interest

The authors have no conflicts to disclose.

DATA AVAILABILITY

The data that support the findings of this study are available from the corresponding author upon reasonable request.

REFERENCES

- ¹Y.-C. Cheng and G. R. Fleming, "Dynamics of light harvesting in photosynthesis," *Annu. Rev. Phys. Chem.* **60**, 241 (2009).
- ²G. D. Scholes, G. R. Fleming, A. Olaya-Castro, and R. van Grondelle, "Lessons from nature about solar light harvesting," *Nat. Chem.* **3**, 763 (2011).
- ³T. Mirkovic, E. E. Ostromov, J. M. Anna, R. van Grondelle, Govindjee, and G. D. Scholes, "Light absorption and energy transfer in the antenna complexes of photosynthetic organisms," *Chem. Rev.* **117**, 249 (2017).
- ⁴V. Krewald, M. Retegan, N. Cox, J. Messinger, W. Lubitz, S. DeBeer, F. Neese, and D. A. Pantazis, "Metal oxidation states in biological water splitting," *Chem. Sci.* **6**, 1676 (2015).
- ⁵H. van Amerongen and R. Croce, "Light harvesting in photosystem II," *Photosynth. Res.* **116**, 251 (2013).
- ⁶R. E. Blankenship, *Molecular Mechanisms of Photosynthesis*, 2nd ed. (Wiley, 2014).
- ⁷N. Kamiya and J.-R. Shen, "Crystal structure of oxygen-evolving photosystem II from Thermosynechococcus vulcanus at 3.7-Å resolution," *Proc. Natl. Acad. Sci. U. S. A.* **100**, 98 (2003).
- ⁸Y. Umena, K. Kawakami, J.-R. Shen, and N. Kamiya, "Crystal structure of oxygen-evolving photosystem II at a resolution of 1.9 Å," *Nature* **473**, 55 (2011).
- ⁹M. L. Groot, J. P. Dekker, R. Van Grondelle, F. T. H. Den Hartog, and S. Völker, "Energy transfer and trapping in isolated photosystem II reaction centers of green plants at low temperature. A study by spectral hole burning," *J. Phys. Chem.* **100**, 11488 (1996).
- ¹⁰T. Renger and E. Schlodder, "Optical properties, excitation energy and primary charge transfer in photosystem II: Theory meets experiment," *J. Photochem. Photobiol. B* **104**, 126 (2011).
- ¹¹D. I. G. Bennett, K. Amarnath, and G. R. Fleming, "A structure-based model of energy transfer reveals the principles of light harvesting in photosystem II supercomplexes," *J. Am. Chem. Soc.* **135**, 9164 (2013).
- ¹²S.-T. Hsieh, L. Zhang, D.-W. Ye, X. Huang, and Y.-C. Cheng, "A theoretical study on the dynamics of light harvesting in the dimeric photosystem II core complex: Regulation and robustness of energy transfer pathways," *Faraday Discuss.* **216**, 94 (2019).
- ¹³F. Mühl and A. Zouni, "Structural basis of light-harvesting in the photosystem II core complex," *Protein Sci.* **29**, 1090 (2020).
- ¹⁴R. Croce and H. van Amerongen, "Light harvesting in oxygenic photosynthesis: Structural biology meets spectroscopy," *Science* **369**, eaay2058 (2020).
- ¹⁵E. Cignoni, V. Slama, L. Cupellini, and B. Mennucci, "The atomistic modeling of light-harvesting complexes from the physical models to the computational protocol," *J. Chem. Phys.* **156**, 120901 (2022).
- ¹⁶G. Raszewski and T. Renger, "Light harvesting in photosystem II core complexes is limited by the transfer to the trap: Can the core complex turn into a photoprotective mode?," *J. Am. Chem. Soc.* **130**, 4431 (2008).
- ¹⁷L. Cupellini, S. Jurinovich, I. G. Prandi, S. Caprasecca, and B. Mennucci, "Photoprotection and triplet energy transfer in higher plants: The role of electronic and nuclear fluctuations," *Phys. Chem. Chem. Phys.* **18**, 11288 (2016).
- ¹⁸V. Mascoli, V. Novoderezhkin, N. Liguori, P. Xu, and R. Croce, "Design principles of solar light harvesting in plants: Functional architecture of the monomeric antenna CP29," *Biochim. Biophys. Acta, Bioenerg.* **1861**, 148156 (2020).
- ¹⁹E. Cignoni, M. Lapillo, L. Cupellini, S. Acosta-Gutiérrez, F. L. Gervasio, and B. Mennucci, "A different perspective for nonphotochemical quenching in plant antenna complexes," *Nat. Commun.* **12**, 7152 (2021).
- ²⁰S. Maity, V. Daskalakis, M. Elstner, and U. Kleinekathöfer, "Multiscale QM/MM molecular dynamics simulations of the trimeric major light-harvesting complex II," *Phys. Chem. Chem. Phys.* **23**, 7407 (2021).
- ²¹M. K. Sener, D. Lu, T. Ritz, S. Park, P. Fromme, and K. Schulten, "Robustness and optimality of light harvesting in cyanobacterial photosystem I," *J. Phys. Chem. B* **106**, 7948 (2002).
- ²²M.-L. Groot, R. N. Frese, F. L. de Weerd, K. Bromek, Å. Pettersson, E. J. G. Peterman, I. H. M. van Stokkum, R. van Grondelle, and J. P. Dekker, "Spectroscopic properties of the CP43 core antenna protein of photosystem II," *Biophys. J.* **77**, 3328 (1999).
- ²³F. L. De Weerd, I. H. M. van Stokkum, H. van Amerongen, J. P. Dekker, and R. van Grondelle, "Pathways for energy transfer in the core light-harvesting complexes CP43 and CP47 of photosystem II," *Biophys. J.* **82**, 1586 (2002).
- ²⁴M. Di Donato, R. van Grondelle, I. H. M. van Stokkum, and M. L. Groot, "Excitation energy transfer in the photosystem II core antenna complex CP43 studied by femtosecond visible/visible and visible/mid-infrared pump probe spectroscopy," *J. Phys. Chem. B* **111**, 7345 (2007).
- ²⁵A. P. Casazza, M. Szczepaniak, M. G. Müller, G. Zucchielli, and A. R. Holzwarth, "Energy transfer processes in the isolated core antenna complexes CP43 and CP47 of photosystem II," *Biochim. Biophys. Acta, Bioenerg.* **1797**, 1606 (2010).
- ²⁶R. Jankowiak, V. Zazubovich, M. Rätsep, S. Matsuzaki, M. Alfonso, R. Picorel, M. Seibert, and G. J. Small, "The CP43 core antenna complex of photosystem II possesses two quasi-degenerate and weakly coupled Q_y -trap states," *J. Phys. Chem. B* **104**, 11805 (2000).
- ²⁷G. Raszewski, W. Saenger, and T. Renger, "Theory of optical spectra of photosystem II reaction centers: Location of the triplet state and the identity of the primary electron donor," *Biophys. J.* **88**, 986 (2005).
- ²⁸V. Zazubovich and R. Jankowiak, "On the energy transfer between quasi-degenerate states with uncorrelated site distribution functions: An application to the CP43 complex of photosystem II," *J. Lumin.* **127**, 245 (2007).
- ²⁹M. Reppert, V. Zazubovich, N. C. Dang, M. Seibert, and R. Jankowiak, "Low-energy chlorophyll states in the CP43 antenna protein complex: Simulation of various optical spectra. II," *J. Phys. Chem. B* **112**, 9934 (2008).
- ³⁰N. C. Dang, V. Zazubovich, M. Reppert, B. Neupane, R. Picorel, M. Seibert, and R. Jankowiak, "The CP43 proximal antenna complex of higher plant photosystem II revisited: Modeling and hole burning study. I," *J. Phys. Chem. B* **112**, 9921 (2008).
- ³¹F. Mühl, M. E.-A. Madjet, and T. Renger, "Structure-based simulation of linear optical spectra of the CP43 core antenna of photosystem II," *Photosynth. Res.* **111**, 87 (2012).
- ³²F. Mühl, M. Plöckinger, H. Ortmayer, M. Schmidt am Busch, D. Lindorfer, J. Adolphs, and T. Renger, "The quest for energy traps in the CP43 Antenna of photosystem II," *J. Photochem. Photobiol. B* **152**, 286 (2015).
- ³³S. Vasil'ev and D. Bruce, "A protein dynamics study of photosystem II: The effects of protein conformation on reaction center function," *Biophys. J.* **90**, 3062 (2006).
- ³⁴S. Maity, A. Gelessus, V. Daskalakis, and U. Kleinekathöfer, "On a chlorophyll-carotenoid coupling in LHCII," *Chem. Phys.* **526**, 110439 (2019).
- ³⁵V. May and O. Kühn, *Charge and Energy Transfer in Molecular Systems*, 3rd ed. (Wiley-VCH, 2011).

- ³⁶A. Damjanović, I. Kosztin, U. Kleinekathöfer, and K. Schulten, "Excitons in a photosynthetic light-harvesting system: A combined molecular dynamics, quantum chemistry and polaron model study," *Phys. Rev. E* **65**, 031919 (2002).
- ³⁷C. Olbrich and U. Kleinekathöfer, "Time-dependent atomistic view on the electronic relaxation in light-harvesting system II," *J. Phys. Chem. B* **114**, 12427 (2010).
- ³⁸C. Olbrich, J. Strümpfer, K. Schulten, and U. Kleinekathöfer, "Theory and simulation of the environmental effects on FMO electronic transitions," *J. Phys. Chem. Lett.* **2**, 1771 (2011).
- ³⁹M. Aghtar, J. Strümpfer, C. Olbrich, K. Schulten, and U. Kleinekathöfer, "Different types of vibrations interacting with electronic excitations in phycoerythrin 545 and Fenna-Matthews-Olson antenna systems," *J. Phys. Chem. Lett.* **5**, 3131 (2014).
- ⁴⁰J. Gao, W.-J. Shi, J. Ye, X. Wang, H. Hirao, and Y. Zhao, "QM/MM modeling of environmental effects on electronic transitions of the FMO complex," *J. Phys. Chem. B* **117**, 3488 (2013).
- ⁴¹S. Shim, P. Rebentrost, S. Valleau, and A. Aspuru-Guzik, "Atomistic study of the long-lived quantum coherences in the Fenna-Matthew-Olson complex," *Biophys. J.* **102**, 649 (2012).
- ⁴²S. Chandrasekaran, M. Aghtar, S. Valleau, A. Aspuru-Guzik, and U. Kleinekathöfer, "Influence of force fields and quantum chemistry approach on spectral densities of BChl a in solution and in FMO proteins," *J. Phys. Chem. B* **119**, 9995 (2015).
- ⁴³S. Jurinovich, L. Viani, C. Curutchet, and B. Mennucci, "Limits and potentials of quantum chemical methods in modelling photosynthetic antennae," *Phys. Chem. Chem. Phys.* **17**, 30783 (2015).
- ⁴⁴M. K. Lee and D. F. Coker, "Modeling electronic-nuclear interactions for excitation energy transfer processes in light-harvesting complexes," *J. Phys. Chem. Lett.* **7**, 3171 (2016).
- ⁴⁵D. Padula, M. H. Lee, K. Claridge, and A. Troisi, "Chromophore-dependent intramolecular exciton-vibrational coupling in the FMO complex: Quantification and importance for exciton dynamics," *J. Phys. Chem. B* **121**, 10026 (2017).
- ⁴⁶C. Curutchet and B. Mennucci, "Quantum chemical studies of light harvesting," *Chem. Rev.* **117**, 294 (2017).
- ⁴⁷C. W. Kim, B. Choi, and Y. M. Rhee, "Excited state energy fluctuations in the Fenna-Matthews-Olson complex from molecular dynamics simulations with interpolated chromophore potentials," *Phys. Chem. Chem. Phys.* **20**, 3310 (2018).
- ⁴⁸B. Mennucci and S. Corni, "Multiscale modelling of photoinduced processes in composite systems," *Nat. Rev. Chem.* **3**, 315 (2019).
- ⁴⁹F. Segatta, L. Cupellini, M. Garavelli, and B. Mennucci, "Quantum chemical modeling of the photoinduced activity of multichromophoric biosystems," *Chem. Rev.* **119**, 9361 (2019).
- ⁵⁰S. Maity, B. M. Bold, J. D. Prajapati, M. Sokolov, T. Kubař, M. Elstner, and U. Kleinekathöfer, "DFTB/MM molecular dynamics simulations of the FMO light-harvesting complex," *J. Phys. Chem. Lett.* **11**, 8660 (2020).
- ⁵¹S. Maity, P. Sarngadharan, V. Daskalakis, and U. Kleinekathöfer, "Time-dependent atomistic simulations of the CP29 light-harvesting complex," *J. Chem. Phys.* **155**, 055103 (2021).
- ⁵²M. Elstner, D. Porezag, G. Jungnickel, J. Elsner, M. Haugk, T. Frauenheim, S. Suhai, and G. Seifert, "Self-consistent-charge density-functional tight-binding method for simulations of complex materials properties," *Phys. Rev. B* **58**, 7260 (1998).
- ⁵³B. M. Bold, M. Sokolov, S. Maity, M. Wanko, P. M. Dohmen, J. J. Kranz, U. Kleinekathöfer, S. Höfener, and M. Elstner, "Benchmark and performance of long-range corrected time-dependent density functional tight binding (LC-TD-DFTB) on rhodopsins and light-harvesting complexes," *Phys. Chem. Chem. Phys.* **22**, 10500 (2020).
- ⁵⁴L. Chen, R. Zheng, Q. Shi, and Y. Yan, "Optical line shapes of molecular aggregates: Hierarchical equations of motion method," *J. Chem. Phys.* **131**, 094502 (2009).
- ⁵⁵A. Ishizaki and G. R. Fleming, "Unified treatment of quantum coherent and incoherent hopping dynamics in electronic energy transfer: Reduced hierarchy equation approach," *J. Chem. Phys.* **130**, 234111 (2009).
- ⁵⁶T. J. Zuehlsdorff, A. Montoya-castillo, J. A. Napoli, T. E. Markland, and C. M. Isborn, "Optical spectra in the condensed phase: Capturing anharmonic and vibronic features using dynamic and static approaches," *J. Chem. Phys.* **151**, 074111 (2019).
- ⁵⁷A. Ishizaki and G. R. Fleming, "On the adequacy of the Redfield equation and related approaches to the study of quantum dynamics in electronic energy transfer," *J. Chem. Phys.* **130**, 234110 (2009).
- ⁵⁸V. I. Novoderezhkin and R. van Grondelle, "Physical origins and models of energy transfer in photosynthetic light-harvesting," *Phys. Chem. Chem. Phys.* **12**, 7352 (2010).
- ⁵⁹T. Renger and F. Mühl, "Understanding photosynthetic light-harvesting: A bottom up theoretical approach," *Phys. Chem. Chem. Phys.* **15**, 3348 (2013).
- ⁶⁰M. Schröder, M. Schreiber, and U. Kleinekathöfer, "A time-dependent modified Redfield theory for absorption spectra applied to light-harvesting systems," *J. Lumin.* **125**, 126 (2007).
- ⁶¹A. Gelzinis, D. Abramavicius, and L. Valkunas, "Absorption lineshapes of molecular aggregates revisited," *J. Chem. Phys.* **142**, 154107 (2015).
- ⁶²T.-C. Dinh and T. Renger, "Lineshape theory of pigment-protein complexes: How the finite relaxation time of nuclei influences the exciton relaxation-induced lifetime broadening," *J. Chem. Phys.* **145**, 034105 (2016).
- ⁶³J. Ma and J. Cao, "Förster resonance energy transfer, absorption and emission spectra in multichromophoric systems. I. Full cumulant expansions and system-bath entanglement," *J. Chem. Phys.* **142**, 094106 (2015).
- ⁶⁴L. Cupellini, F. Lipparini, and J. Cao, "Absorption and circular dichroism spectra of molecular aggregates with the full cumulant expansion," *J. Phys. Chem. B* **124**, 8610 (2020).
- ⁶⁵B. Webb and A. Sali, "Comparative protein structure modeling using MODELLER," *Curr. Protoc. Bioinf.* **54**, 5 (2016).
- ⁶⁶S. Jo, T. Kim, V. G. Iyer, and W. Im, "CHARMM-GUI: A web-based graphical user interface for CHARMM," *J. Comput. Chem.* **29**, 1859 (2008).
- ⁶⁷L. Zhang, D.-A. Silva, Y. Yan, and X. Huang, "Force field development for cofactors in the photosystem II," *J. Comput. Chem.* **33**, 1969 (2012).
- ⁶⁸A. W. Sousa da Silva and W. F. Vranken, "ACPPPE-Antechamber Python parser interface," *BMC Res. Notes* **5**, 367 (2012).
- ⁶⁹C. Olbrich, J. Strümpfer, K. Schulten, and U. Kleinekathöfer, "Quest for spatially correlated fluctuations in the FMO light-harvesting complex," *J. Phys. Chem. B* **115**, 758 (2011).
- ⁷⁰M. Gaus, A. Goez, and M. Elstner, "Parametrization and benchmark of DFTB3 for organic molecules," *J. Chem. Theory Comput.* **9**, 338 (2013).
- ⁷¹T. Kubař, K. Welke, and G. Groenhof, "New QM/MM implementation of the DFTB3 method in the gromacs package," *J. Comput. Chem.* **36**, 1978 (2015).
- ⁷²B. Hourahine, B. Aradi, V. Blum, F. Bonafé, A. Buccheri, C. Camacho, C. Cevallos, M. Y. Deshaye, T. Dumitrić, A. Dominguez, S. Ehler, M. Elstner, T. Van Der Heide, J. Hermann, S. Irle, J. Kranz, C. Köhler, T. Kowalczyk, T. Kubař, I. S. Lee, V. Lutsker, R. J. Maurer, S. K. Min, I. Mitchell, C. Negre, T. A. Niehaus, A. M. N. Niklasson, A. J. Page, A. Pecchia, G. Penazzi, M. P. Persson, J. Režáč, C. G. Sánchez, M. Sternberg, M. Stöhr, F. Stuckenber, A. Tkatchenko, V. W.-Z. Yu, and T. Frauenheim, "DFTB+, a software package for efficient approximate density functional theory based atomistic simulations," *J. Chem. Phys.* **152**, 124101 (2020).
- ⁷³J. J. Kranz, M. Elstner, B. Aradi, T. Frauenheim, V. Lutsker, A. D. Garcia, and T. A. Niehaus, "Time-dependent extension of the long-range corrected density functional based tight-binding method," *J. Chem. Theory Comput.* **13**, 1737 (2017).
- ⁷⁴G. S. Engel, T. R. Calhoun, E. L. Read, T.-K. Ahn, T. Mančal, Y.-C. Cheng, R. E. Blankenship, and G. R. Fleming, "Evidence for wavelike energy transfer through quantum coherence in photosynthetic systems," *Nature* **446**, 782 (2007).
- ⁷⁵C. Olbrich, T. L. C. Jansen, J. Liebers, M. Aghtar, J. Strümpfer, K. Schulten, J. Knoester, and U. Kleinekathöfer, "From atomistic modeling to excitation transfer and two-dimensional spectra of the FMO light-harvesting complex," *J. Phys. Chem. B* **115**, 8609 (2011).
- ⁷⁶L. Zhang, D.-A. Silva, H. Zhang, A. Yue, Y. Yan, and X. Huang, "Dynamic protein conformations preferentially drive energy transfer along the active chain of the photosystem II reaction centre," *Nat. Commun.* **5**, 4170 (2014).
- ⁷⁷N. Liguori, X. Periole, S. J. Marrink, and R. Croce, "From light-harvesting to photoprotection: Structural basis of the dynamic switch of the major antenna complex of plants (LHCII)," *Sci. Rep.* **5**, 15661 (2015).

- ⁷⁸M. Aghtar, U. Kleinekathöfer, C. Curutchet, and B. Mennucci, "Impact of electronic fluctuations and their description on the exciton dynamics in the light-harvesting complex PE545," *J. Phys. Chem. B* **121**, 1330 (2017).
- ⁷⁹J. Adolphs, F. Mühl, M. E.-A. Madjet, and T. Renger, "Calculation of pigment transition energies in the fmo protein: From simplicity to complexity and back," *Photosynth. Res.* **95**, 197 (2008).
- ⁸⁰J. Adolphs, F. Mühl, M. E.-A. Madjet, M. Schmidt am Busch, and T. Renger, "Structure-based calculations of optical spectra of photosystem I suggest an asymmetric light-harvesting process," *J. Am. Chem. Soc.* **132**, 3331 (2010).
- ⁸¹C. Curutchet, G. D. Scholes, B. Mennucci, and R. Cammi, "How solvent controls electronic energy transfer and light harvesting: Toward a quantum-mechanical description of reaction field and screening effects," *J. Phys. Chem. B* **111**, 13253 (2007).
- ⁸²G. D. Scholes, C. Curutchet, B. Mennucci, R. Cammi, and J. Tomasi, "How solvent controls electronic energy transfer and light harvesting," *J. Phys. Chem. B* **111**, 6978 (2007).
- ⁸³T. Renger and F. Mühl, "Theory of excitonic couplings in dielectric media: Foundation of Poisson-TrEsp method and application to photosystem I trimers," *Photosynth. Res.* **111**, 47 (2012).
- ⁸⁴M. Schröder, U. Kleinekathöfer, and M. Schreiber, "Calculation of absorption spectra for light-harvesting systems using non-Markovian approaches as well as modified Redfield theory," *J. Chem. Phys.* **124**, 084903 (2006).
- ⁸⁵J. Cao, R. J. Cogdell, D. F. Coker, H.-G. Duan, J. Hauer, U. Kleinekathöfer, T. L. C. Jansen, T. Mančal, R. J. D. Miller, J. P. Ogilvie, V. I. Prokhorenko, T. Renger, H.-S. Tan, R. Tempelaar, M. Thorwart, E. Thyraug, S. Westenhoff, and D. Zigmantas, "Quantum biology revisited," *Sci. Adv.* **6**, eaaz4888 (2020).
- ⁸⁶L. Cupellini and F. Lipparini (2020). "FCE program to compute optical spectra with the full cumulant expansion," OpenAIRE. [10.5281/ZENODO.3900199](https://doi.org/10.5281/ZENODO.3900199)
- ⁸⁷V. I. Novoderezhkin, M. A. Palacios, H. van Amerongen, and R. van Grondelle, "Energy-transfer dynamics in the LHCII complex of higher plants: Modified Redfield approach," *J. Phys. Chem. B* **108**, 10363 (2004).
- ⁸⁸V. I. Novoderezhkin, M. A. Palacios, H. van Amerongen, and R. van Grondelle, "Excitation dynamics in the LHCII complex of higher plants: Modeling based on the 2.72 Å crystal structure," *J. Phys. Chem. B* **109**, 10493 (2005).
- ⁸⁹F. Mühl, M. E.-A. Madjet, and T. Renger, "Structure-based identification of energy sinks in plant light-harvesting complex II," *J. Phys. Chem. B* **114**, 13517 (2010).
- ⁹⁰D. Loco, S. Jurinovich, L. Cupellini, M. F. S. J. Menger, and B. Mennucci, "The modeling of the absorption lineshape for embedded molecules through a polarizable QM/MM approach," *Photochem. Photobiol. Sci.* **17**, 552 (2018).
- ⁹¹V. Sláma, L. Cupellini, and B. Mennucci, "Exciton properties and optical spectra of light harvesting complex II from a fully atomistic description," *Phys. Chem. Chem. Phys.* **22**, 16783 (2020).
- ⁹²O. Rancova and D. Abramavicius, "Static and dynamic disorder in bacterial light-harvesting complex LH2: A 2DES simulation study," *J. Phys. Chem. B* **118**, 7533 (2014).
- ⁹³D. Loco and L. Cupellini, "Modeling the absorption lineshape of embedded systems from molecular dynamics: A tutorial review," *Int. J. Quantum Chem.* **119**, e25726 (2018).
- ⁹⁴A. Singhary, C. Maffeo, K. H. Delgado-Magnero, D. J. K. Swainsbury, M. Sener, U. Kleinekathöfer, J. W. Vant, J. Nguyen, A. Hitchcock, B. Isralewitz, I. Teo, D. E. Chandler, J. E. Stone, J. C. Phillips, T. V. Pogorelov, M. I. Mallus, C. Chipot, Z. Luthey-Schulten, D. P. Tielemans, C. N. Hunter, E. Tajkhorshid, A. Aksimentiev, and K. Schulten, "Atoms to phenotypes: Molecular design principles of cellular energy metabolism," *Cell* **179**, 1098 (2019).